Materials and Design 173 (2019) 107764

Contents lists available at ScienceDirect

Materials and Design

journal homepage: www.elsevier.com/locate/matdes

Hardness and corrosion behaviour of anodised Al-Si produced by rheocasting

Baiwei Zhu *, Caterina Zanella

Department of Materials and Manufacturing, School of Engineering, Jönköping University, P.O. Box 1026, Gjuterigatan 5, SE-551 11 Jönköping, Sweden

HIGHLIGHTS

- •Fe-intermetallics dissolved partly during anodising, leaving vacancies as defects remain in the oxide layer.
- The longitudinal macrosegregation influences the corrosion protection of the oxide layer but does not affect its hardness.
- The surface liquid segregation (SLS) layer on rheocasting behaves as a skin effect on the as-cast surface.
- Higher oxide thickness decreases the hardness and corrosion resistance of the oxide layer.

GRAPHICAL ABSTRACT

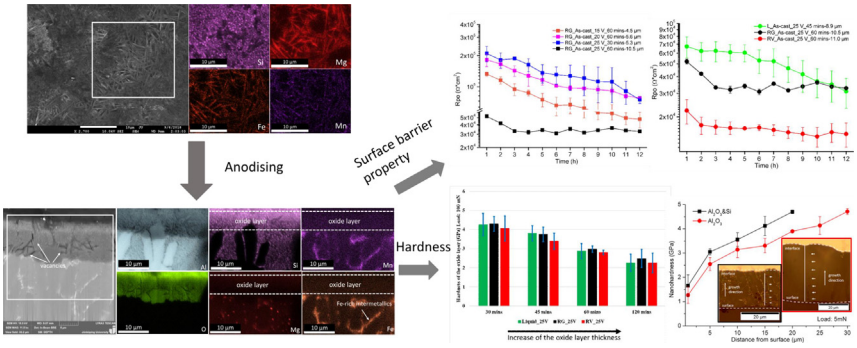

ARTICLE INFO

Article history:
Received 15 November 2018
Received in revised form 8 March 2019
Accepted 26 March 2019
Available online 28 March 2019

Keywords:
Rheocasting
Anodising
Al oxide layer
Corrosion protection
Surface layer segregation

ABSTRACT

The anodised layer of Al-Si alloys produced by rheocasting was studied and compared to anodised traditional liquid casting in this paper. The anodising was performed in 1.0 M H_2SO_4 solution at room temperature on the as-cast substrates, and anodising voltage and time were optimised as process parameters. This study focuses on understanding the effect of the surface liquid segregation (SLS) layer by rheocasting on the hardness and corrosion protection of the oxide layer. The hardness depends on the anodising parameters and varies along the oxide thickness. The corrosion protection given by the oxide layer was evaluated by electrochemical impedance spectroscopy (EIS) in 3 wt-% NaCl solution, and the results revealed that the longitudinal macrosegregation influences the corrosion protection, with the near-to-vent region showing lower corrosion protection due to a higher eutectic fraction. A comparison between liquid and rheocast samples indicated that the presence of SLS layer by the transverse macrosegregation does not have a significant impact on the corrosion resistance of the oxide layer. Moreover, it was found that an increase of the oxide layer thickness by longer anodising time or higher applied voltage decreases both the hardness and corrosion resistance of the oxide layer.

1. Introduction

With the growing demand of light aluminium castings in automotive and electronic industries, semi-solid metal (SSM) process such as rheocasting, is now more and more used to produce near net shape components of Al-Si alloys. SSM process takes advantages of the production of components with improved mechanical properties due to the lower shrinkage and gas porosity defects, as well as the possibility to perform T6 heat treatment [1–3]. However, the SSM process increases the microstructural inhomogeneity in the cast component due to the presence of a slurry and the consequent separation of the solid

* Corresponding author.
E-mail address: Baiwei.Zhu@ju.se (B. Zhu).

https://doi.org/10.1016/j.matdes.2019.107764

particles from the liquid phase during the filling of the mould. This leads to both a longitudinal and transverse macrosegregation. The liquid phase flows faster further from the gating system, and therefore higher liquid fraction can be found in the region near to the vent (longitudinal macrosegregation) or in the surface of the component compared to the core (transverse macrosegregation) [4,5]. Transverse macrosegregation creates a surface liquid segregation (SLS) layer which has higher eutectic fraction and precipitates, as the liquid phase is enriched in alloying elements. The increase of eutectic fraction and precipitates were expected to affect the surface properties. Previous studies indicated that the presence of SLS layer contributes to an improvement of surface hardness [6,7] and has an impact on the corrosion behaviour of cast components [8–12]. In the work of Möller et al. [12], the semi-solid cast component with the SLS layer shows a higher corrosion rate than the component without the SLS layer. However, Eslami et al. [10] indicated that the SLS layer promotes the corrosion resistance mainly due to surface defects, and polishing of surface improves the corrosion resistance compared to the as-cast condition.

Even though Al-Si alloys are difficult to be anodised, anodising is still used to improve the corrosion and wear resistance for the application in harsh environments as well as increasing surface hardness. A limited number of studies have proved that the oxide layer and its performance on cast aluminium alloys are strongly affected by chemical composition [13–15], microstructure [13–15], manufacturing process [16–19], pretreatment [16], the anodising parameters [20,21] and post-treatment [22]. In a previous work by Zhu et al. [14,15], it was found that the presence of Al-Si eutectic region results in a localised thinning of the oxide layer where the corrosion attack initiates. Therefore, in the particular case of semi-solid cast Al alloys, the SLS layer is expected to have a significant influence on the anodising performance. Few previous research considered the SLS layer on components during anodising and reported that the presence of the SLS layer results in a thin and porous layer with worse corrosion resistance [16,17]. However, a deeper understanding of the influence of the SLS layer on the oxide growth and its corrosion resistance is needed.

This paper aims to investigate the hardness and the corrosion behaviour of anodised Al-Si substrate produced by rheocasting and to understand the influence of the casting method, segregation, and the anodising processes parameters on the final properties. A traditional liquid casting with the same composition is tested as a reference.

2. Experimental

2.1. Materials and casting

An EN AC 42000 Al alloy with an addition of 150 ppm Sr was used in this study (chemical composition is reported in Table 1). Sr is added in order to modify the Si particle morphology in the eutectic region from the typically interconnected plates to more disconnected fibres. This modification has been proven to be beneficial to improve the quality of the anodised layer [14,15]. The rheocasting process applied in this study is the RheoMetal™ [23] process. The slurry was prepared with the stirring speed around 1000 rpm and 35 °C of superheat (melt temperature before slurry making at 650 °C). The solid fraction (primary α-Al phases) in the slurry was controlled by the amount of enthalpy exchange material (EEM), and EEM to shot melt ratio was fixed to 7 wt% in this study thus obtaining 46% of primary α-Al solid fraction [24]. The prepared slurry was then poured into the shot sleeve of a vertical pressure die casting (VPDC) machine to cast in 10 mm thick samples with the geometry shown in Fig. 1. Machine parameters such as die temperature, plunger advance speed and intensification pressure, were kept constant at 175 °C, 0.3 m/s and 160 bar, respectively. Prior to liquid and semi-solid casting, 10 liquid shots were performed to heat up the machine and maintain the thermal conditions in the shot sleeve and die cavity. In this study, rheocast parts taken from near to the gate and near to the vent were chosen for benchmarking, as shown in Fig. 1.

Table 1
Chemical composition of EN AC 42000 ingots.

Alloy	Si	Mg	Cu	Fe	Mn	Zn	Sr
Average value [wt-%]	7.000	0.380	0.074	0.400	0.260	0.065	0.015
Standard deviation	0.030	0.007	0.001	0.003	0.002	0.001	0.001

2.2. Anodising

Prior to anodising, Al-Si samples in as-cast condition were ultrasonically cleaned in ethanol for 5 min. The anodising process was carried out in 1.0 M H_2SO_4 solution at room temperature in a cell with an inner diameter of 100 mm. A conductive oxide with a size of 10 × 10 mm^2 was used as a cathode with a distance of 40 mm to the Al-Si sample. In this study, three constant voltage, 15 V, 20 V and 25 V, were applied, and the duration of anodising time was varied from 15 min to 120 min. After anodising, samples were ultrasonically rinsed in distilled water for 3 min and dried at 50 °C for 30 min. The previous study by Zhu et al. revealed that the hydrothermal sealing could generate cracks into the oxide layer, leading to a reduced corrosion protection of the oxide layer in Al-Si alloys [25]. Therefore, in this study, no sealing step was employed.

2.3. Microstructural characterisation

A diamond saw was used to cut the anodised samples with low speed and low load to avoid damaging the oxide layer when preparing the samples. The microstructure was studied by optical microscopy (OM, Olympus GX71F) and scanning electron microscopy (SEM, JEOL JSM-7001F) equipped with energy dispersive X-ray spectroscopy (EDXS). OM was also employed to measure the oxide layer thickness in the cross-section. For the measurement of the oxide layer thickness, 5 different areas were selected in each sample, and at least 8 measurements were performed on each area on a regular space distance. A Tescan focused-ion-beam SEM (FIB-SEM) was applied to characterise the anodised layer before and after corrosion in the cross-section.

2.4. Hardness testing

The hardness of the anodised layer was determined by Micro Materials NanoTest™ Vantage equipped with Berkovich indenter. The load for surface hardness testing was set at 100 mN to avoid measuring the hardness of the Al-Si substrate, while the load for the profile hardness measurements in the cross-section was 5 mN. Moreover, the hardness of the Al-Si substrates was measured as reference by applying 100 mN load.

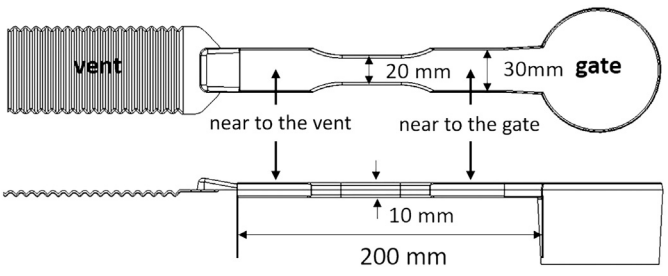

Fig. 1. Sketch of the cast component.

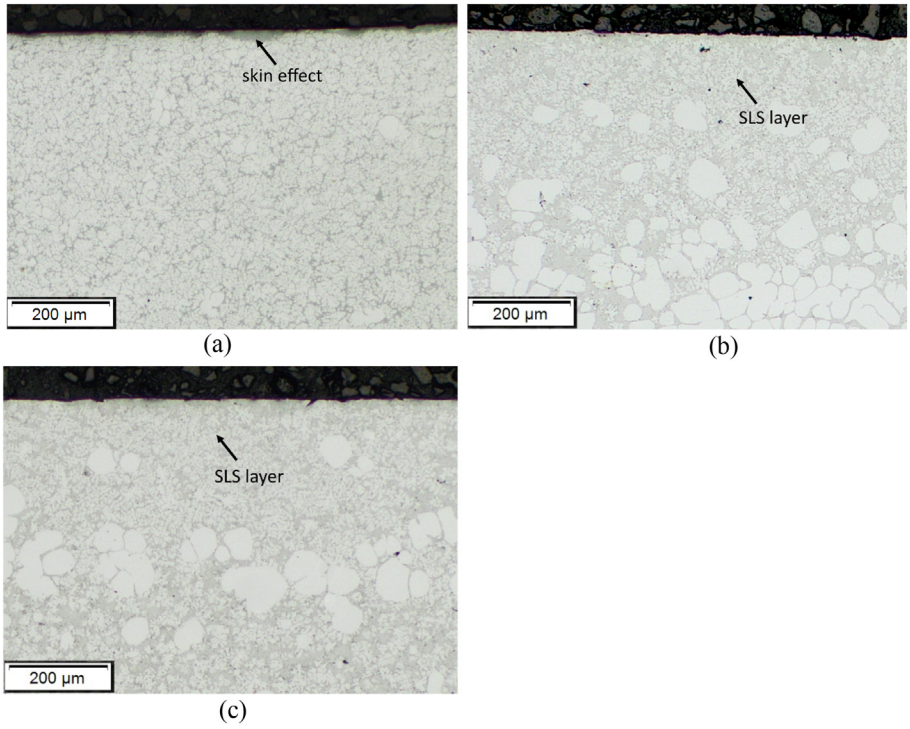

Fig. 2. Micrographs obtained near the casting surface for (a) liquid casting, (b) rheocasting, near to the gate, (c) rheocasting, near to the vent.

2.5. Corrosion testing

Electrochemical impedance spectra of selected samples were collected by using a three-electrode configuration with a Pt ring and an Ag/AgCl electrode (3 M KCl) as counter and reference electrodes, respectively, on an Ivium Vertex potentiostat. The spectra were collected during 12 h of immersion in 3 wt-% NaCl solution. The frequency ranged from 10^{-1} Hz to 10^{5} Hz with 30 points and amplitude of the sinusoidal potential is 15 mV at open-circuit potential. In this study, at least three measurements of the same type of sample have been performed to ensure the repeatability. The collected impedance data were analysed and fitted by ZSimp Win software.

3. Results and discussion

3.1. Microstructure of Al-Si substrates

The liquid casting substrate has the typical dendritic microstructure (Fig. 2a), while on the contrary, the microstructure of rheocast Al-Si alloys (Fig. 2b–c) shows the presence of spherical primary α-Al particles surrounded by smaller secondary α-Al phases and Al-Si eutectic regions and intermetallics. Fig. 2b–c demonstrates the presence of the SLS layer which contains a higher fraction of Al-Si eutectic regions and Fe-rich intermetallics both in near-to-gate and near-to-vent parts. Moreover, comparing the microstructure of parts near to the gate and near to the vent, it is visible that more Al-Si eutectic regions segregate to the part at near to the vent proving that the liquid fraction flows further in the mould leading to longitudinal segregation. [4].

Differently from most of the previous studies, the as-cast surface of castings was investigated in this study by SEM equipped with EDXS. The chemical composition of cast surface on different positions was measured by EDXS (Table 2) in the top view, and the results show much higher alloying elements on the surface than the composition of the ingots (Table 1). Fig. 3 reports the as-cast surfaces of liquid sample and rheocast sample taken from near to the gate. It is noticeable that the as-cast surfaces of both liquid and rheocast samples are enriched with eutectic regions and Fe-intermetallics. In liquid casting, the surface alloying element enrichment (as shown in Table 2) was expected due to the skin effect [26] and the segregation by a combination of inverse segregation and exudation [27]. The higher alloying elements and therefore more eutectic regions on the surface of rheocast samples were associated with transverse macrosegregation due to the rheocasting process.

3.2. Oxide layer characterisation

An oxide layer was generated on the Al-Si substrates by anodising with a combination of different voltage values and time. The cross-section microstructures of selected anodised layers are presented in Fig. 4. Si particles remain embedded in the oxide layer as they do not dissolve and only oxidise very little during the anodising [15]. A comparison of the microstructure of anodised layers on the liquid cast sample (Fig. 4a) and on the rheocast sample (Fig. 4b) shows that more Si particles remain embedded in the oxide layer on the rheocast sample, due to the presence of SLS layer. The microstructural characterisation of bulk EN AC 42000 substrates revealed the presence of Fe-rich intermetallics. However, as shown in Fig. 4, no Fe-intermetallics were evident in the oxide layer. FIB-SEM analysis was performed to investigate

Table 2
Surface chemical composition of rheocast samples in different locations and liquid samples by EDXS.

Casting method		Si	Mg	Fe	Mn	Cu	Al
Rheocast	Near to the gate	17.65 ± 0.38	2.09 ± 0.11	1.18 ± 0.11	0.59 ± 0.08	0.09 ± 0.05	Bal.
	Near to the vent	18.17 ± 0.39	1.99 ± 0.09	1.39 ± 0.11	0.62 ± 0.04	0.10 ± 0.04	Bal.
Liquid		15.46 ± 0.73	1.79 ± 0.11	0.79 ± 0.17	0.37 ± 0.09	0.04 ± 0.03	Bal.

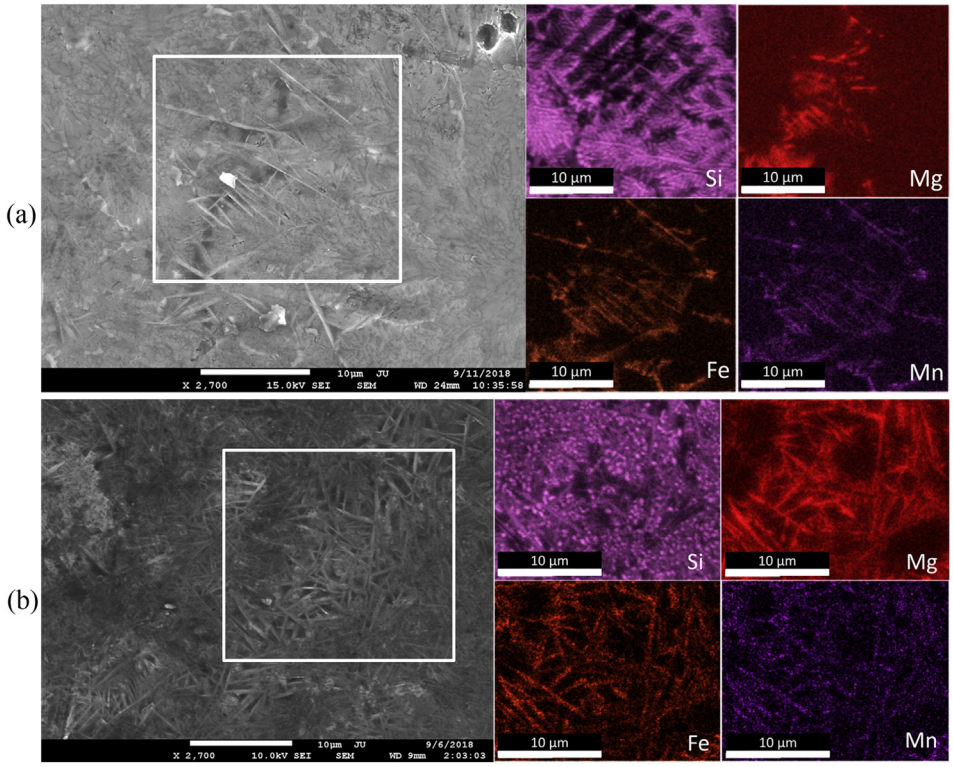

Fig. 3. SEM micrographs and EDXS elemental mapping of as-cast surface on (a) full liquid sample, and (b) rheocast sample taken from near to the gate.

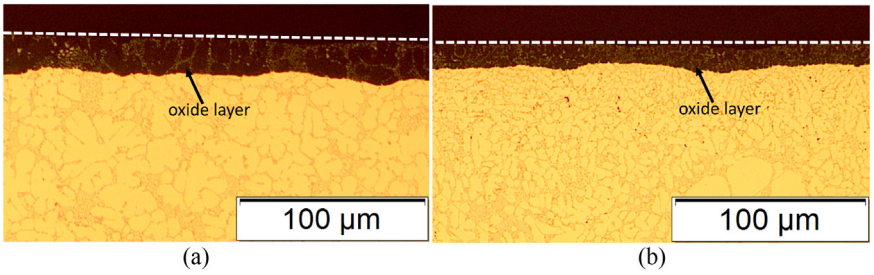

Fig. 4. Micrograph of the oxide layer (anodising at 25 V for 60 min) on (a) liquid cast sample; (b) as-cast rheocast sample, near to gate.

the oxide layer in more detail without introducing extra damage during the sample preparation. The embedded fibrous Si particles and cracks/vacancies in the oxide layer are shown in Fig. 5. As shown in Fig. 5, the EDXS elemental mapping identified fibrous Si particles, as well as few Fe-rich intermetallics and Mg_2Si in Al-Si substrates, while no Fe-intermetallics or Mg_2Si were revealed in the oxide layer. Instead of Fe-intermetallics, voids with a similar geometry and layout of Fe-intermetallics were evident. A similar result was also reported in the previous work by Zhu et al. [28]. Depending on the chemical composition and density, the Fe-rich intermetallics can be completely or partly dissolved during anodising [29,30].

Fig. 6a summarises the measured average thickness of the oxide layer of all samples as a function of anodising time at a constant voltage of 25 V. The standard deviation (green) and minimum value (white) are

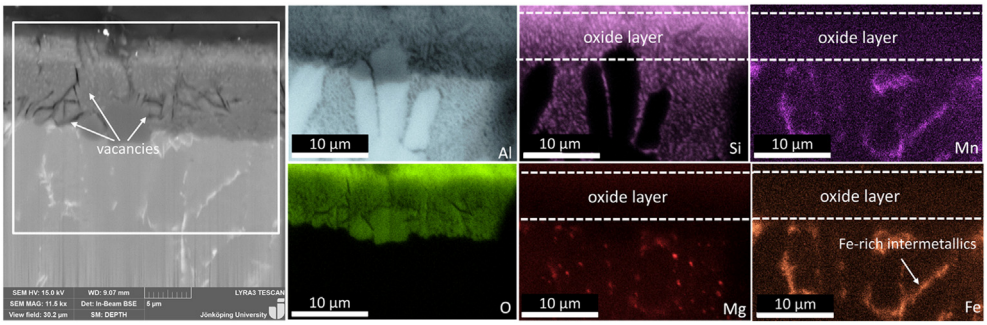

Fig. 5. FIB-SEM micrographs and EDXS elemental mapping of the oxide layer on the rheocast sample anodised at 25 V for 60 min.

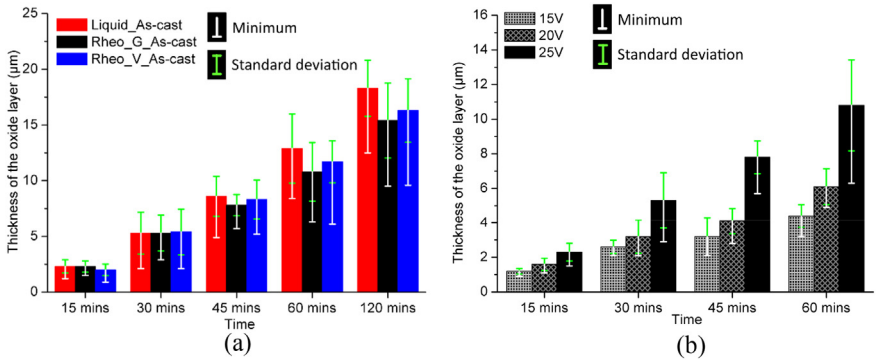

Fig. 6. Thickness of the oxide layer (a) all sample condition at 25 V, (b) 15, 20 and 25 V, near-to-gate part in as-cast condition. (For interpretation of the references to color in this figure, the reader is referred to the web version of this article.)

represented as error bars. As shown in Fig. 6a, the average thickness as well as minimum thickness increase with the increase of anodising time. A more detailed explanation is given in [28]. The relation between the oxide layer thickness and the anodising voltage of the rheocast part is depicted in Fig. 6b. An increase in voltage significantly increases the average thickness and minimum thickness of the oxide layer. Similar results were also reported by Nickel et al. [31] and Kuhn et al. [32], and Li et al. reported that by anodising under voltage control, the current density increased exponentially with the applied voltage [33]. The growth of the oxide layer is driven by the ion transport, where Al^{3+} moves outwards while the O^{2-} migrate into the oxide layer. A high voltage increases ionic transportation, thus, the high oxide growth rate, as well as a thicker oxide layer, was obtained by increasing applied voltage.

3.3. Hardness of the oxide layer

3.3.1. The effect of casting method and macrosegregation on the hardness of the oxide layer

The hardness of Al-Si substrates and anodised layer with anodising time from 30 min to 120 min at 25 V has been measured and presented in Fig. 7. As expected, the anodised layer exhibits a much higher hardness than Al-Si substrates. The hardness results indicate that the casting method and longitudinal macrosegregation do not have a significant influence on the hardness of both the Al-Si substrates and the anodised surface, despite the rheocast sample have more eutectic regions on the surface. A previous study by Fratila-Apachitei et al. [34] indicates that Si has a slightly detrimental effect on microhardness of the anodised layer by comparing the oxide layer in the pure Al and Al-Si substrates. In the anodising of Al-Si alloys containing Fe-intermetallics, a higher Si level in Al-Si alloys can result in a higher fraction of eutectic region in the oxide layer with an increased number of defects [14], and increased number of Fe-intermetallics would probably introduce more voids. Hence, the decreased value of oxide layer hardness in term of rheocast sample especially near-to-vent sample could be expected due to the more defective oxide layer by transverse and longitudinal macrosegregation. However, due to the limited enrichment of alloying elements (Table 2), the transverse and longitudinal macrosegregation in rheocast samples may be insufficient to have an evident detrimental effect on the hardness of the anodised layer.

3.3.2. The effect of anodising time on the hardness of the oxide layer

In this study, samples anodised at 25 V were selected to study the influence of anodising time on the hardness of the oxide layer, as a larger range of anodising time was performed in 25 V condition. It was found that the anodising time has a significant influence on the hardness of the oxide layer. As shown in Fig. 7, the values of the hardness of the oxide

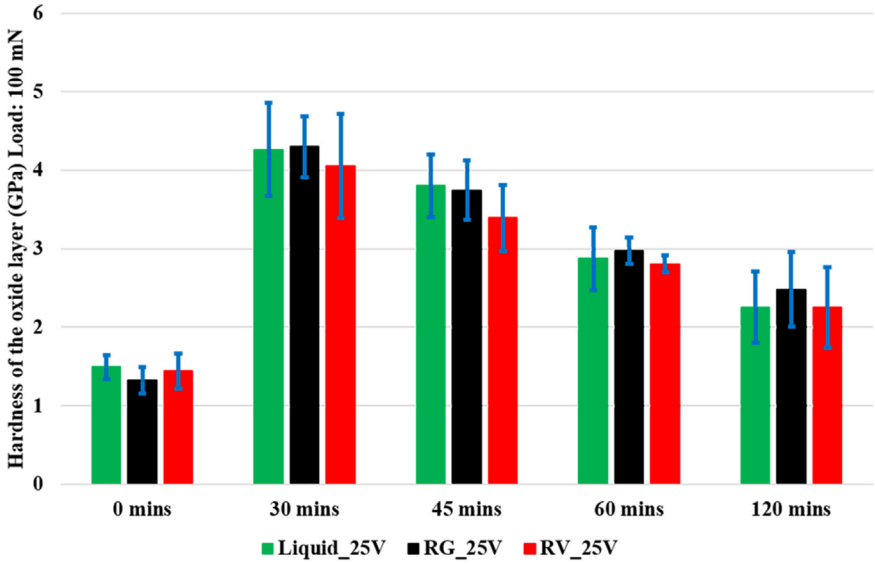

Fig. 7. Surface hardness of Al-Si substrates and anodised layer on cast samples at 25 V.

layer decrease with increasing of anodising time on both liquid and rheocast samples. A similar result was also reported in the previous study by Rasmussen [35], and it was related to the increase of bath temperature over time. In the current study, the bath temperature was controlled between 22 and 25 °C, but the local heating effect on the sample surface during anodising is very likely due to the resistive effect of the growing oxide. Fig. 8 reports the nanohardness profile along the cross-section of the oxide layer as a function of the distance to the surface. The local hardness of the oxide layer shows a continuous increase from the surface to the substrate/oxide interface. A previous study by Aerts et al. [36] indicated a more porous oxide structure near the surface due to the effect of thermally enhanced oxide dissolution on the oxide surface with increasing electrolyte temperature and time of exposure to the electrolyte. In the current study, the aluminium oxide close to the surface, forming earlier than the aluminium oxide near the interface, is longer affected by the local heating effect and might result in an oxide with larger nanoporosity and therefore slightly lower hardness. The same effect explains the relationship among oxide hardness values and anodising time. The longer the oxide is exposed to the heating effect, the larger the porous structure of the oxide becomes.

Furthermore, the decrease of oxide layer hardness with increasing anodising time could also be related to the defects in the oxide layer. In the anodising of Al-Si alloys, the volume expansion by forming aluminium oxide could result in intrinsic stress, especially near the Si particles [15]. As a result of stress release after anodising, the defect would be introduced in the oxide layer. More oxide layer defects would be generated when the oxide layer thickness increases, resulting in the degradation of oxide layer hardness.

3.3.3. The effect of the applied voltage on the hardness of the oxide layer

The influence of the applied voltage on the hardness of the oxide layer was also investigated in this study. Fig. 9 describes the hardness of the oxide layer formed at different voltages with similar oxide layer thickness by the nanoindentation technique. When produced at the same thickness (different anodising time), a similar hardness of the oxide layer is obtained despite the applied voltages are different. Higher voltage should increase the heating effect, but this is compensated by the lower anodising time. Therefore, it could be concluded that the oxide layer thickness determines the hardness of the oxide layer.

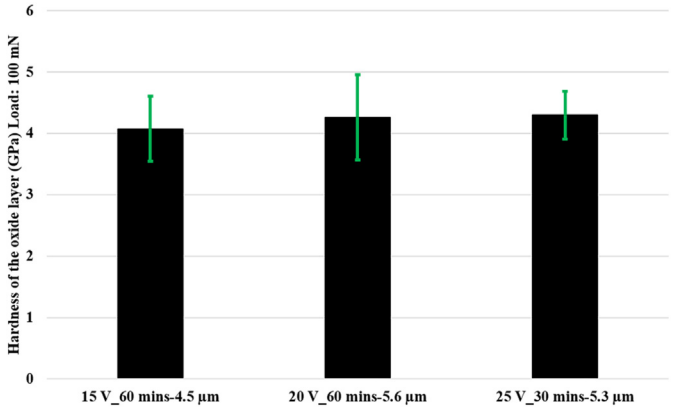

Fig. 9. Surface hardness of the oxide layer anodising at 15, 20, 25 V with similar thickness.

3.4. Electrochemical characterisation

3.4.1. The effect of the casting method and the longitudinal macrosegregation on the corrosion resistance of the oxide layer

Samples with a comparable oxide thickness of 10 µm, anodised at 25 V were tested by EIS monitoring the barrier properties over a 12 hour immersion period in 3 wt-% NaCl. Samples produced by liquid casting or rheocasting with different position related to the gate were compared. Fig. 10 shows the open-circuit potential (OCP) values for measured samples with a function of immersion time. As shown in Fig. 10, the OCP values for liquid samples and rheocast samples taken from near to the gate decreases in the first 4 h and then remained stable, while the OCP values for the rheocast sample from near to the vent were stable with the immersion time. The Bode plots of EIS spectra of selected samples obtained after 1, 4, 8 and 12 h of immersion in 3wt-% NaCl solution were reported in Fig. 11 (Nyquist plots of selected anodised samples are attached in the Supplement). Generally, the results show that

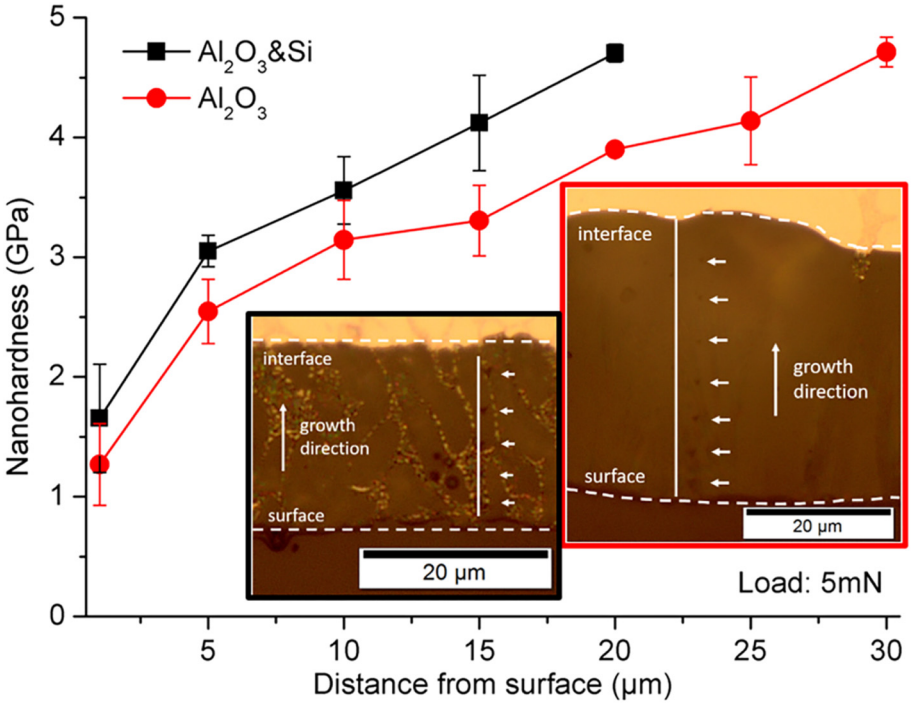

Fig. 8. Hardness of the oxide layer (5 mN) with a function of the distance to the surface on the rheocast sample with anodising at 25 V for 120 min by using nanoindentation.

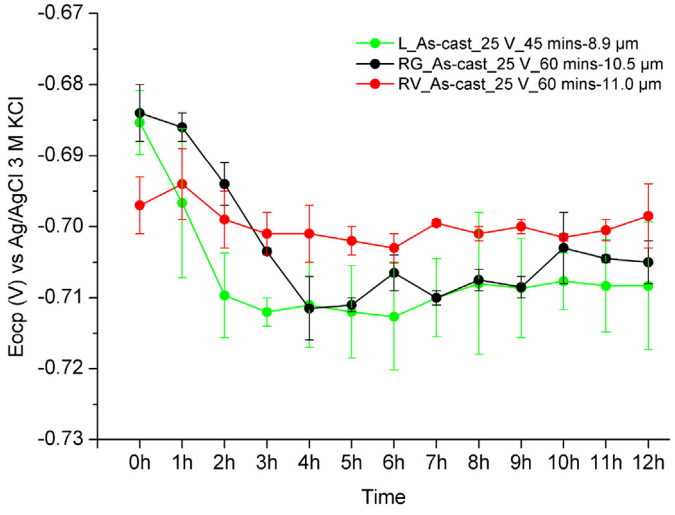

Fig. 10. Open circuit potential (OCP) values as function of immersion time for liquid and rheocast samples.

the total impedance modulus decreases, and the phase angle depresses with the immersion time, which demonstrates a progressive corrosion attack.

Comparing the impedance spectra of liquid cast samples and rheocast samples after anodising, the liquid cast sample shows slightly higher impedance modulus at low frequencies before 8 h of immersion. Regarding the effect of different locations on impedance spectra, parts taken from near to the gate depict relatively higher impedance values at the low frequencies, compared to parts from near to the vent.

To obtain quantitative results regarding the corrosion resistance of the anodised layer, impedance spectra were fitted by the equivalent circuits, $R_{el}(CPE_{ox}R_{ox})(CPE_{in}R_{po})$ and $R_{el}(CPE_{ox}(R_{ox}(CPE_{in}R_{po})))$. Similar equivalent circuits were applied previously [10,14]. In circuits, R_{el} indicates the resistance of the electrolyte, while R_{ox} and R_{po} stand for the resistance of the oxide layer and the polarisation resistance, respectively [14]. Two constant phase elements (CPE), CPE_{ox} and CPE_{in} were used to simulate the capacitive behaviour of the oxide layer and the electrical double layer, respectively [14]. Fig. 11 depicts measured (points) and fitting (grey lines) spectra of measured samples where the good fitting is evident. The evolution of average polarisation resistance (R_{po}) in anodised samples, as well as average "pre-factor" Q_{in}, were summarised in Fig. 12 with error bar referring to the standard deviation, and Table 3 presents the changing values of n for CPE_{in} over time. As shown in Fig. 12, the values of R_{po} decrease, while the corresponding values of Q_{in} tend to increase, which indicate a localised attack [10,37].

In general, R_{po} shows relative low values for an anodised surface, proving the presence of some defects in the oxide. Comparing the fitting results of liquid cast and rheocast samples, it appears that the liquid cast sample has a slightly higher value of R_{po} than rheocast samples. The presence of the SLS layer, known as transverse macrosegregation, was believed to hinder the corrosion resistance of the anodised surface on rheocast samples, due to the significant amount of eutectic regions in the oxide layer [17] and the consequent defects formation. However, the difference is not much. Both samples show low resistance due to the skin effect as well as segregation in the liquid cast component and the SLS layer in the rheocast sample locally, which leads to a similar corrosion protection performance of the oxide layer as it on the rheocast sample at near to the gate.

Samples taken from different locations exhibit variations in R_{po} and Q_{in} values regarding the anodised Al-Si alloys by rheocasting. As shown in Fig. 12, the anodised sample taken from near to the gate obtains relatively higher values of R_{po} and lower values of Q_{in} than the sample from near to the vent. Microstructural observation of Al-Si substrates by OM showed that the longitudinal macrosegregation leads to a relatively higher Si level increasing the Al-Si eutectic fraction near to the vent. The presence of more Al-Si regions makes the oxide layer more defective, facilitating the propagation of the corrosion attack [14].

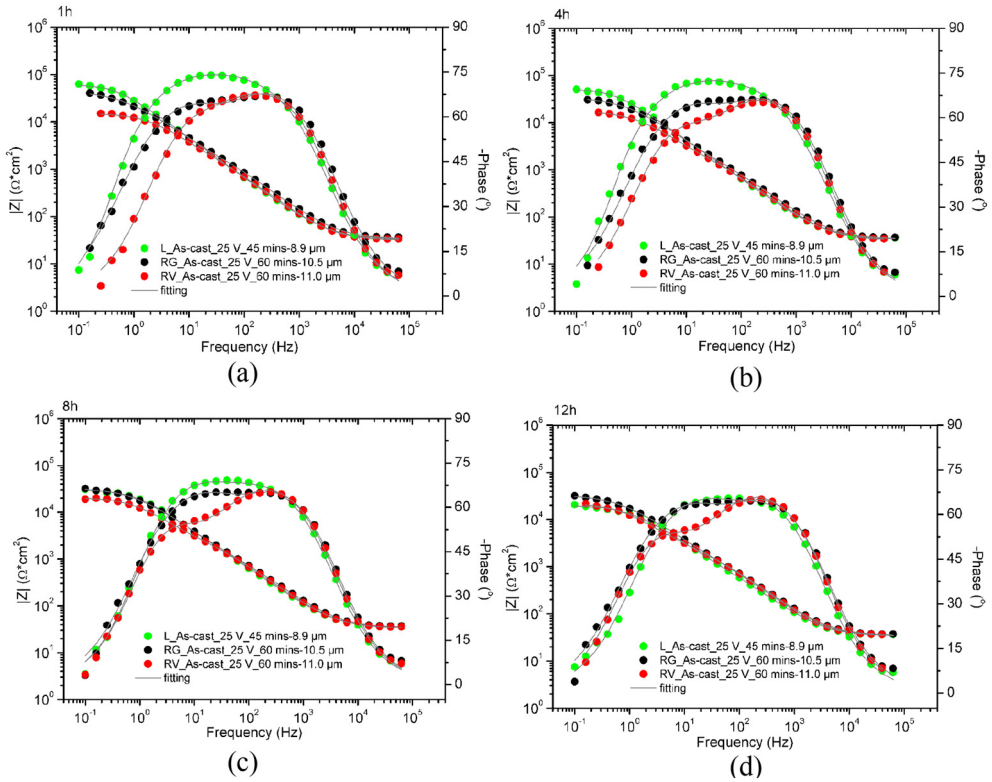

Fig. 11. Bode plots of impedance spectra of selected anodised samples after (a) 1 h; (b) 4 h; (c) 8 h and (d) 12 h of immersion.

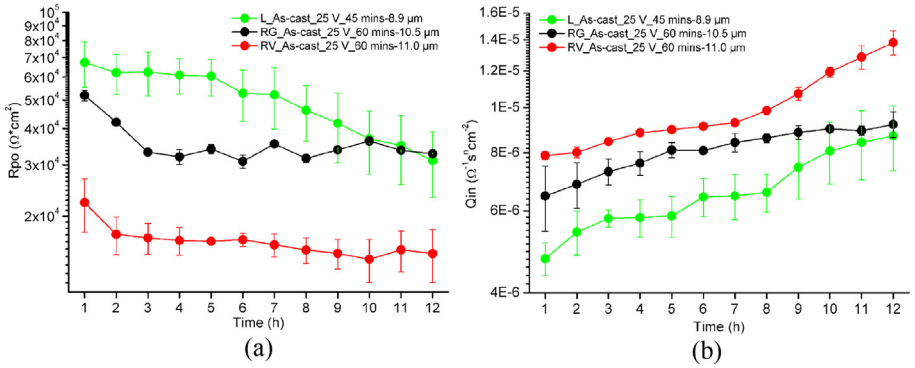

Fig. 12. Results of equivalent circuits fitting for selective material, (a) R_{po}; (b) Q_{in}.

Moreover, judging from Table 2, a relatively higher level of Fe in the sample from near to the vent might result in an increase of Fe-intermetallics in the microstructure. After anodising, an increasing number of vacancies as defects derived from the dissolution of Fe-intermetallics are present in the oxide layer, which could be a result of lower corrosion protection performance in the anodised sample from near to the vent. The similar results were also presented in works by Wu et al. [38] and Zhang et al. [39].

3.4.2. The effect of anodising time and applied voltage on the corrosion resistance of the oxide layer

The effect of anodising time and applied voltage on the corrosion resistance of the oxide layer rheocast samples anodised with similar oxide thickness were tested by EIS. The OCP values reported in Fig. 13 show that anodised samples with oxide layer thickness around 5 µm show stable OCP values with the immersion time. The OCP values of the anodised sample with thicker oxide layer thickness decreases in the first 4 h and then remains stable. Fig. 14 depicts the Bode plot of EIS spectra of selected anodised samples after 1, 4, 8 and 12 h of immersion in 3 wt-% NaCl solution (Nyquist plots of selected anodised samples were attached in the Supplement). As shown in Fig. 14, the total impedance modulus decreases, and the phase angle depresses with the immersion time. A comparison of the EIS spectra of rheocast samples anodised at 15, 20 and 25 V for 60 min reveals that the rheocast samples anodised at 15 and 20 V obtain higher impedance modulus at low frequency than sample anodising at 25 V. Moreover, comparing the impedance spectra of rheocast samples anodising at 25 V for 30 min and 60 min, it was found that, at low frequency, the total impedance modulus of sample anodised for 30 min is higher than that of sample anodised for 60 min.

Similarly, impedance spectra of anodised samples were fitted by the equivalent circuit, $R_{el}(CPE_{ox}R_{ox})(CPE_{in}R_{po})$, and a good match of fitted (grey lines) and measured (points) spectra is evident in Fig. 14. The evolution of average polarisation resistance (R_{po}) of the oxide layer, and average "pre-factor" Q_{in} with standard deviation as the error bar are presented in Fig. 15, and the values of n for CPE_{in} over time is reported in Table 4.

The fitting results show that the anodising time and therefore the oxide thickness has a significant influence on the corrosion resistance of the oxide layer. In Fig. 15, a comparison of fitting results of samples anodised at 25 V for 30 and 60 min shows that the sample anodised for 30 min is associated with higher R_{po} values and lower Q_{in} values than sample anodised for 60 min. As depicted in Fig. 6b, the samples anodised at 25 V for 30 and 60 min obtain the oxide layer with average thicknesses of 5.3 and 10.5 µm, respectively. The resistance values initially increase with the oxide thickness as it could be expected, but after a maximum at 30 min/5 µm, the resistance decreases for thicker coatings. As previously discussed, the increase of the anodising time increases the thickness of the oxide layer, and it could generate more intrinsic stress in the oxide layer during the anodising of Al-Si alloys. With the release of the stress after anodising, more defects would be introduced in the oxide layer, resulting in the degradation of the corrosion protection [14,15].

Table 3
Values of n for CPE_{in} for tested materials.

Materials	Value of n for CPE_{in} with 12 h
L_As-Cast_25 V_45 min-8.9 µm	0.81–1
RG_As-cast_25 V_60 min-10.5 µm	0.71–0.80
RV_As-cast_25 V_60 min-11.0 µm	0.85–1

3.5. Corrosion attack characterisation

Selected corroded anodised surface from cast sample was analysed by SEM equipped with an EDXS and was reported in Fig. 16. As shown in Fig. 16, the surface suffers from an intensive localised corrosion attack of the oxide layer grown on the eutectic region. The corrosion propagation path was revealed by applying FIB-SEM in a cross-section view, as shown in Fig. 17. The corrosion attack initiates from the surface of the eutectic region and propagates through the eutectic region where the Si particles may have some defects with surrounded Al_2O_3 matrix. These results are in accordance with results of the work by Zhu et al. [14].

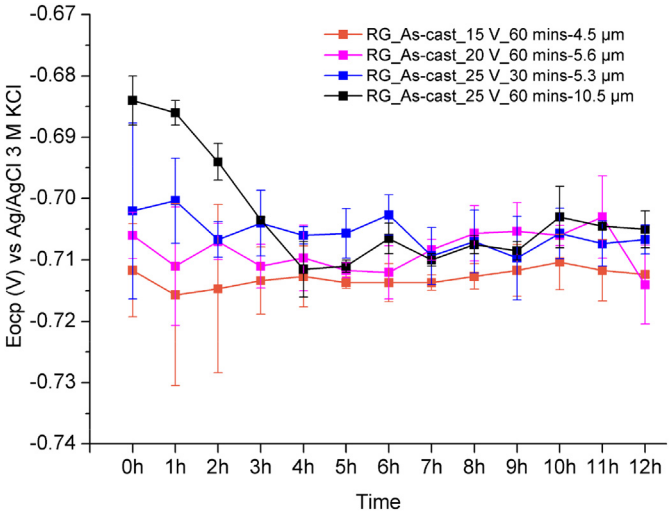

Fig. 13. The OCP values as a function of immersion time for rheocast samples anodising at 15 V, 20 V and 25 V for 60 min and at 25 V for 30 min.

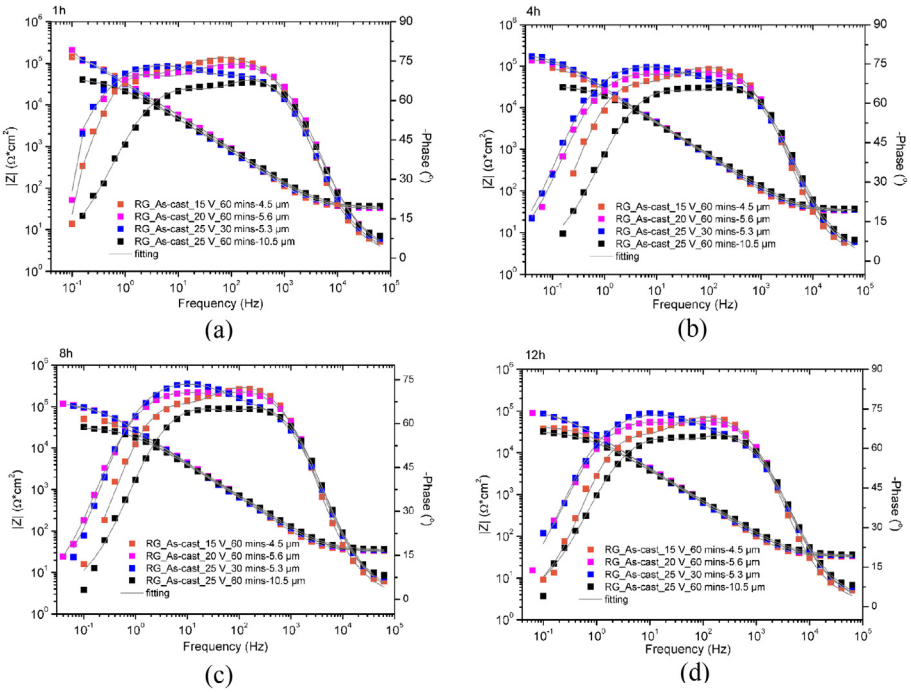

Fig. 14. Bode plots of impedance spectra of selected rheocast samples anodising at 15 V, 20 V and 25 V for 60 min and at 25 V for 30 min after (a) 1 h; (b) 4 h; (c) 8 h and (d) 12 h of immersion.

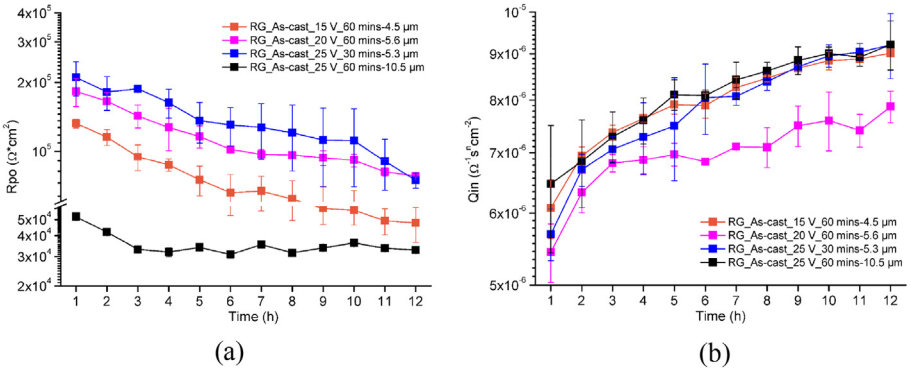

Fig. 15. Representative results of equivalent circuits fitting for selective anodised samples, (a) R_{po}; (b) Q_{in}.

4. Conclusion

In this paper, the anodising behaviour of Al-Si components produced by liquid casting and rheocasting was studied and compared. Second phase particles in the eutectic region such as the Si particle and the Fe-intermetallic play as different roles during anodising. Si particles remain embedded in the oxide layer, while the Fe-rich intermetallics are dissolved which makes the oxide layer defective.

The anodising parameters, such as anodising time and applied voltage, influence the hardness and corrosion resistance of the oxide layer.

Table 4
Values of n for CPE_{in} for selective anodised samples.

Selective anodised samples	Value of n for CPE_{in} with 12 h
RG_As-cast_15 V_60 min-4.5 μm	0.86–0.96
RG_As-cast_20 V_60 min-5.6 μm	0.83–0.90
RG_As-cast_25 V_30 min-5.3 μm	0.85–0.91
RG_As-cast_25 V_60 min-10.5 μm	0.71–0.80

For Al-Si alloys, an increase of the layer thickness could result in more stress introduced defects in the oxide layer, as well as larger nanoporosity in the oxide microstructure due to a local heating effect. Thus, an increase of the oxide layer thickness by increasing anodising time or applied voltage decreases the hardness and corrosion resistance of the oxide layer.

The corrosion resistance of the oxide layer on Al-Si components is strongly influenced by the microstructure of the substrate as well as on the oxide thickness, in which the eutectic region plays an important role. The eutectic region acts as a propagation path for the corrosion attack. More eutectic regions, as well as cracks and defects derived from the dissolution of Fe-rich intermetallics, facilitate the propagation of corrosion attack.

In this study, the longitudinal macrosegregation due to the rheocasting process was evaluated in terms of corrosion resistance and hardness. The longitudinal macrosegregation influences the corrosion protection provided by the oxide layer, with the part at near to the vent showing lower corrosion protection due to a higher eutectic fraction on the surface. However, the longitudinal macrosegregation does not have a significant impact on the hardness of the rheocast Al-

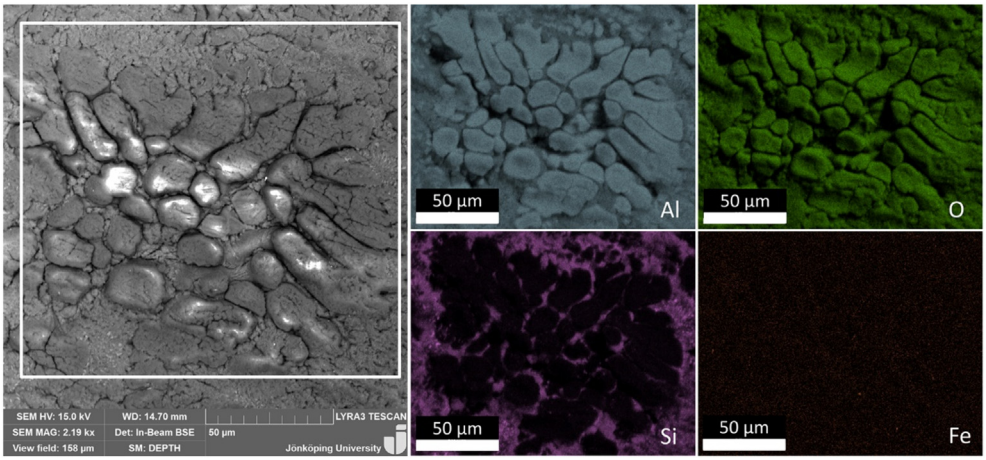

Fig. 16. SEM micrographs and EDXS elemental mapping of the corroded surface in anodised sample by liquid casting.

Si components before or after anodising. The presence of SLS layer by the transverse macrosegregation due to the rheocasting process does not have a significant impact on the corrosion behaviour of the oxide layer of as-cast surfaces compared to liquid casting, as the liquid casting has a skin effect on the as-cast surface.

CRediT authorship contribution statement

Baiwei Zhu: Conceptualization, Data curation, Investigation, Writing - original draft. **Caterina Zanella:** Conceptualization, Supervision, Writing - review & editing.

Acknowledgements

This research work was supported by the KK-foundation (CompCast, Project No. 20100280, and CompCast Plus, Project No. 20170066), who is gratefully acknowledged. The authors would like to thank Jorge Santos for his assistance with casting experiments and Dr. Nils-Eric Andersson for his assistance with FIB-SEM analysis.

Appendix A. Supplementary data

Supplementary data to this article can be found online at https://doi.org/10.1016/j.matdes.2019.107764.

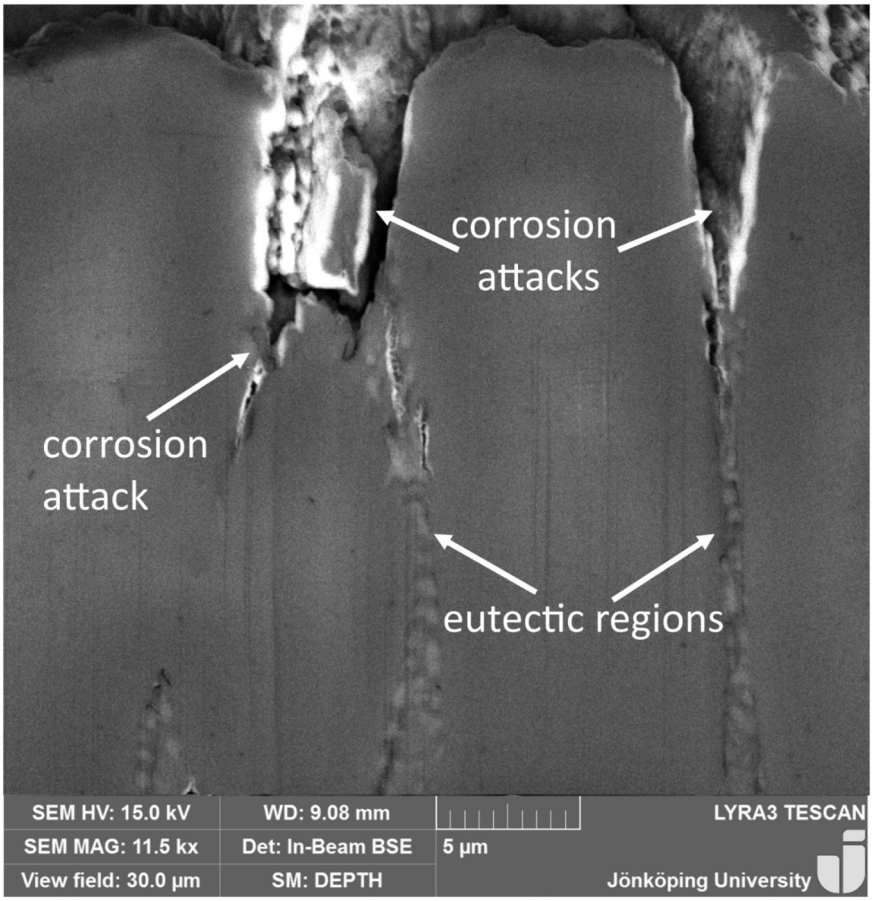

Fig. 17. FIB-SEM micrograph of the corroded area in cross-section taken from the anodised sample by liquid casting.

References

[1] H.V. Atkinson, Semisolid processing of metallic materials, Mater. Sci. Technol. 26 (12) (2010) 1401–1413.
[2] D. Brabazon, D.J. Browne, A.J. Carr, Mechanical stir casting of aluminium alloys from the mushy state: process, microstructure and mechanical properties, Mater. Sci. Eng. A 326 (2) (2002) 370–381.
[3] Y.B. Yu, P.Y. Song, S.S. Kim, J.H. Lee, Possibility of improving tensile strength of semi-solid processed A356 alloy by a post heat treatment at an extremely high temperature, Scr. Mater. 41 (7) (1999) 767–771.
[4] H. Kaufmann, W. Franger, U. Galovsky, P.J. Uggowitzer, Fluctuations of alloy composition and their influence on sponge effect and fluidity of A356-NRC, in: H. Kaufmann (Ed.), 2nd International Light Metals Technology Conference, LKR-Verlag, St. Wolfgang, Austria 2005, pp. 169–177.
[5] H.I. Laukli, C.M. Gourlay, A.K. Dahle, Migration of crystals during the filling of semi-solid castings, Metall. Mater. Trans. A 36 (3) (2005) 805–818.
[6] G. Govender, H. Möller, Evaluation of surface chemical segregation of semi-solid cast aluminium alloy A356, Solid State Phenom. 141-143 (2008) 433–438.
[7] H. Möller, U.A. Caurle, E.P. Masuku, Characterization of surface liquid segregation in SSM-HPDC aluminium alloys, Trans. Nonferrous Metals Soc. China 20 (2010) 847–851.
[8] R. Arrabal, B. Mingo, A. Pardo, M. Mohedano, E. Matykina, I. Rodríguez, Pitting corrosion of rheocast A356 aluminium alloy in 3.5 wt.% NaCl solution, Corros. Sci. 73 (2013) 342–355.
[9] J.M. Bastidas, A. Forn, M.T. Baile, J.L. Polo, C.L. Torres, Pitting corrosion of A357 aluminium alloy obtained by semisolid processing, Mater. Corros. 52 (2001) 691–696.
[10] M. Eslami, M. Payandeh, F. Deflorian, A.E.W. Jarfors, C. Zanella, Effect of segregation and surface condition on corrosion of rheo-HPDC Al–Si alloys, Metals 8 (4) (2018) 209–226.
[11] B. Mingo, R. Arrabal, A. Pardo, E. Matykina, P. Skeldon, 3D study of intermetallics and their effect on the corrosion morphology of rheocast aluminium alloy, Mater. Charact. 112 (2016) 122–128.
[12] H. Möller, E.P. Masuku, The influence of liquid surface segregation on the pitting corrosion behavior of semi-solid metal high pressure die cast alloy F357, Open Corros. J. 2 (2009) 216–220.
[13] L.E. Fratila-Apachitei, H. Terryn, P. Skeldon, G.E. Thompson, J. Duszczyk, L. Katgerman, Influence of substrate microstructure on the growth of anodic oxide layers, Electrochim. Acta 49 (2004) 1127–1140.
[14] B. Zhu, M. Fedel, N.-E. Andersson, P. Leisner, F. Deflorian, C. Zanella, Effect of Si content and morphology on corrosion resistance of anodized cast Al-Si alloys, J. Electrochem. Soc. 164 (7) (2017) C435–C441.
[15] B. Zhu, S. Seifeddine, P.O.Å. Persson, A.E.W. Jarfors, P. Leisner, C. Zanella, A study of formation and growth of the anodised surface layer on cast Al-Si alloys based on different analytical techniques, Mater. Des. 101 (2016) 254–262.
[16] K. Chauke, H. Möller, U.A. Curle, G. Govender, Anodising of Al-Mg-Si-(Cu) alloys produced by R-HPDC, Mater. Sci. Forum 765 (2013) 658–662.
[17] L. Chaukea, K. Mutombo, G. Govender, Corrosion behaviour of the anodised A356 aluminium alloy produced by the rheo-high pressure die casting process, Adv. Mater. Res. 1019 (2014) 67–73.
[18] F. Riddar, S. Hogmark, Å. Kassman Rudolphi, Comparsion of anodised aluminium surface from four fabrication methods, J. Mater. Process. Technol. 212 (2012) 2272–2281.
[19] R.I. Revilla, D. Verkens, G. Couturiaux, L. Malet, L. Thijs, S. Godet, I. De Graeve, Galvanostatic anodizing of additive manufactured Al-Si10-Mg alloy, J. Electrochem. Soc. 164 (14) (2017) C1027–C1034.
[20] L.E. Fratila-Apachitei, I. Apachitei, J. Duszczyk, Thermal effects associated with hard anodizing of cast aluminum alloys, J. Appl. Electrochem. 36 (2006) 481–486.
[21] T. Tamamoto, H. Tanaka, M. Fujita, H. Asoh, S. Ono, Effect of high-frequency switching electrolysis on film thickness uniformity of anodic oxide film formed on AC8A aluminum alloy, J. Jpn. Inst. Light Metals 60 (11) (2010) 602–607.
[22] M. Mohedano, E. Matykina, R. Arrabal, B. Mingo, A. Pardo, PEO of pre-anodized Al–Si alloys: corrosion properties and influenceof sealings, Appl. Surf. Sci. 346 (2015) 57–67.
[23] M. Wessén, H. Cao, The RSF technology – a possible breakthrough for semi-solid casting processes, J. Metallur. Sci. Technol. 25 (2) (2007) 22–28.
[24] J. Santos, A.E.W. Jarfors, A.K. Dahle, Filling, feeding and defect formation of thick-walled AlSi7Mg0.3 semi-solid castings, Solid State Phenom. 256 (2016) 222–227.
[25] B. Zhu, M. Fedel, N.-E. Andersson, P. Leisner, F. Deflorian, C. Zanella, Influence of the Sr modification and post-treatment on corrosion resistance of oxide layer of cast Al-(low)Si alloys, Joint European Corrosion Congress 2017, EUROCORR 2017 and 20th International Corrosion Congress and Process Safety Congress 2017, Asociace koroznich inzenyru z.s.- AKI - Czech Association of Corrosion Engineers, Prague, Czech Republic 2017, pp. 27–39.
[26] Z.W. Chen, Skin solidification during high pressure die casting of Al–11Si–2Cu–1Fe alloy, Mater. Sci. Eng. A 348 (1–2) (2002) 145–153.
[27] S. Otarawanna, C.M. Gourlay, H.I. Laukli, A.K. Dahle, Microstructure formation in AlSi4MgMn and AlMg5Si2Mn high-pressure die castings, Metall. Mater. Trans. A 40 (7) (2009) 1645–1659.
[28] B. Zhu, S. Seifeddine, A.E.W. Jarfors, P. Leisner, C. Zanella, A study of anodising behaviour of Al-Si components produced by rheocasting, 15th International Conference on Semi-solid Processing of Alloys and Composites, Shenzhen, China, 2018.
[29] M. Jariyaboon, P. Møller, R.E. Dunin-Borkowski, R. Ambat, FIB-SEM investigation of trapped intermetallic particles in anodic oxide films on AA1050 aluminium, Anti-Corros. Methods Mater. 58 (4) (2011) 173–178.
[30] K. Shimizu, G.M. Brown, K. Kobayashi, P. Skeldon, G.E. Thompson, G.C. Wood, Ultramicrotomy—a route towards the enhanced understanding of the corrosion and filming behaviour of aluminium and its alloys, Corros. Sci. 40 (7) (1998) 1049–1072.
[31] D. Nickel, D. Dietrich, R. Morgenstern, I. Scharf, H. Podlesak, T. Lampke, Anodisation of aluminium alloys by micro-capillary technique as a tool for reliable, cost-efficient, and quick process parameter determination, Adv. Mater. Sci. Eng. 2016 (2016) (12 pages).
[32] D. Kuhn, A. Martin, C. Eckart, M. Sieber, R. Morgenstern, M. Hackert-Oschätzchen, T. Lampke, A. Schubert, Localised anodic oxidation of aluminium material using a continuous electrolyte jet, 2017 IOP Conf. Ser.: Mater. Sci. Eng. IOP Publishing Ltd, Chemnitz, Germany, 2017.
[33] F. Li, L. Zhang, R.M. Metzger, On the growth of highly ordered pores in anodized aluminum oxide, Chem. Mater. 10 (1998) 2470–2480.
[34] L.E. Fratila-Apachitei, J. Duszczyk, L. Katgerman, Vickers microhardness of AlSi(Cu) anodic oxide layers formed in H_2SO_4 at low temperature, Surf. Coat. Technol. 165 (2003) 309–315.
[35] J. Rasmussen, New insights into the microhardness of anodized aluminum, Met. Finish. 99 (9) (2001) 46–51.
[36] T. Aerts, T. Dimogerontalis, I. De Graeve, J. Fransaer, H. Terryn, Influence of the anodizing temperature on the porosity and the mechanical properties of the porous anodic oxide film, Surf. Coat. Technol. 201 (2007) 7310–7317.
[37] J.A. Moreto, C.E.B. Marina, W.W. Bose Fiho, L.A. Rocha, J.C.S. Fernandes, SVET, SKP and EIS study of the corrosion behaviour of high strength Al and Al–Li alloys used in aircraft fabrication, Corros. Sci. 84 (2014) 30–41.
[38] H. Wu, Y. Ma, W. Huang, X. Zhou, K. Li, Y. Liao, Z. Wang, Z. Liang, L. Liu, Effect of iron-containing intermetallic particles on film structure and corrosion resistance of anodized AA2099 alloy, J. Electrochem. Soc. 165 (9) (2018) C573–C581.
[39] F. Zhang, J.-O. Nilsson, J. Pan, In situ and operando AFM and EIS studies of anodization of Al 6060: influence of intermetallic particles, J. Electrochem. Soc. 163 (9) (2016) C609–C618.